Cancer Imaging (2012) **12,** 153–162
DOI: 10.1102/1470-7330.2012.0016

CI

e-med
www.e-med.org.uk

REVIEW

Pheochromocytoma and paraganglioma: imaging characteristics

Juan C. Baez[a], Jyothi P. Jagannathan[b], Katherine Krajewski[b], Kevin O'Regan[b], Katherine Zukotynski[b], Matthew Kulke[b], Nikhil H. Ramaiya[b]

[a]*Department of Radiology, Brigham and Women's Hospital, Boston, MA, USA;* [b]*Department of Imaging, Dana-Farber Cancer Institute, Boston, MA, USA*

Corresponding address: Juan Carlos Baez, 75 Francis St., Boston, MA 02115, USA.
Email: jcbaez@gmail.com

Date accepted for publication 27 January 2012

Abstract

The accurate diagnosis of adult pheochromocytoma and paraganglioma necessitates a multidisciplinary approach that includes clinical history, biochemical testing, and multimodality imaging such as computed tomography, magnetic resonance imaging, and nuclear medicine studies. This review illustrates the different imaging characteristics of primary adult pheochromocytomas as well as both sympathetic and parasympathetic paragangliomas. The review also describes known genetic associations and shows common metastatic patterns. Knowledge of the diverse appearance of pheochromocytomas and paragangliomas can result in early initial diagnosis or detection of disease recurrence thereby affecting patient management and prognosis.

Keywords: *Pheochromocytoma; paraganglioma; multiple endocrine neoplasia.*

Introduction

Neural crest cells constitute a multipotent population from which numerous cellular lineages including melanocytes, craniofacial cartilage and bone, smooth muscle, neurons, and glia as well as tumors such as pheochromocytomas, paragangliomas, and neuroblastomas arise. Pheochromocytoma cells differentiate from epinephrine secreting, neural crest-derived, precursor cells of the adrenal medulla[1]. Paraganglia cells also originate from the neural crest, but differentiate into sympathetic and parasympathetic subtypes that can give rise to paragangliomas. Sympathetic paragangliomas secrete norepinephrine; parasympathetic paragangliomas are nonsecretory and typically occur in the head and neck[2]. Pheochromocytomas and paragangliomas are rare tumors with a combined annual incidence of less than 1 in 300,000[2]. Traditionally, pheochromocytomas are described by the rule of 10s where 10% are metastatic, 10% are bilateral, 10% are familial, 10% are extraadrenal (paragangliomas), and 10% are not associated with hypertension[2]. Although the rule of 10s is a helpful approximation, current research has stressed the increased importance of genetic predisposition in the development of pheochromocytomas and paragangliomas. Furthermore, the rate of metastases varies widely depending on the tumor origin[3]. Only 2–10% of pheochromocytomas metastasize compared with 20–70% of extraadrenal paragangliomas[3].

The diagnosis of pheochromocytoma and paraganglioma depends on the clinical history, the presence of urinary or circulating catecholamines/metabolites, imaging findings, and tissue histopathology. Patients can be asymptomatic or symptomatic, presenting with episodic hypertension, tachycardia, palpitations, perspiration, pallor, headache, and nonspecific abdominal or flank pain[2]. Although pheochromocytomas and paragangliomas can have similar clinical and radiologic features, these tumors differ in prognosis and likelihood of metastatic spread[4,5].

This pictorial review demonstrates the common imaging characteristics of pheochromocytomas and paragangliomas using multiple imaging modalities and describes some common genetic syndrome associations. Since the anatomic location of the tumor changes the prognosis, numerous sites of both adrenal and extraadrenal tumors

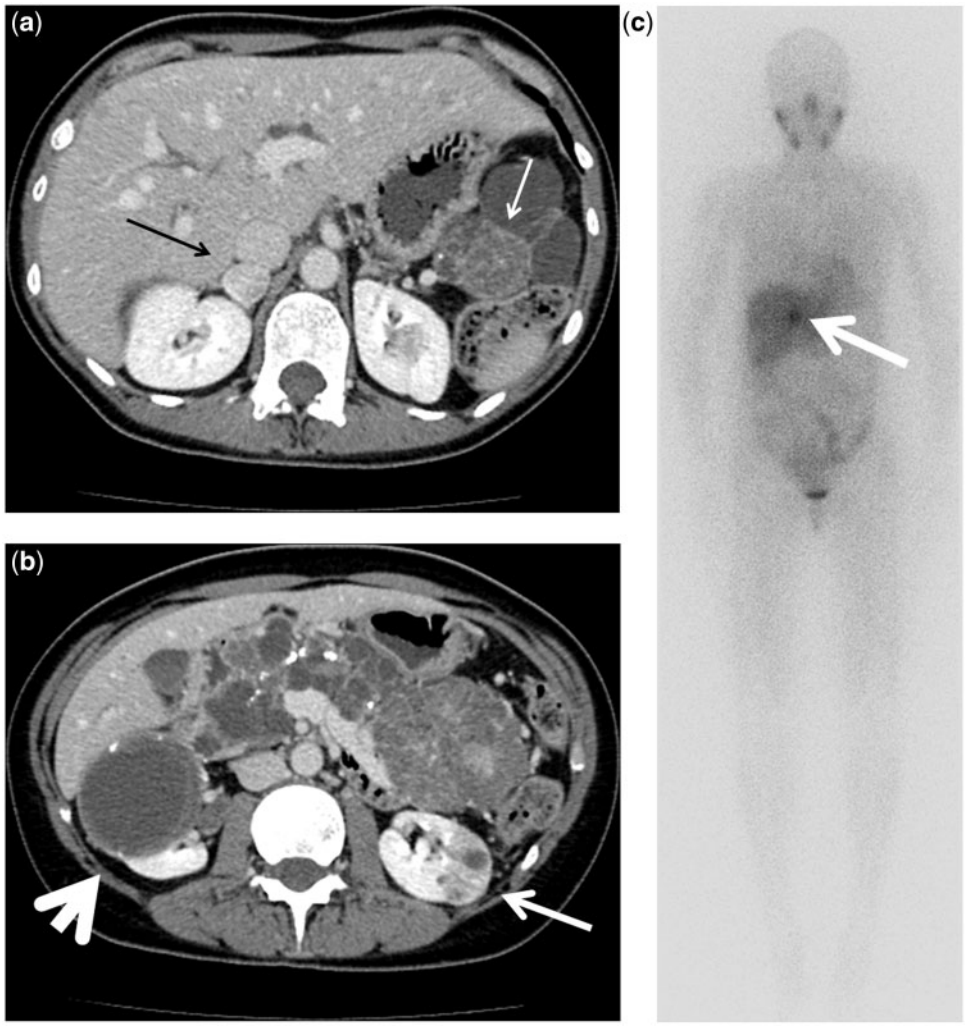

Figure 1 **A 41-year-old woman with a history of Von Hippel-Lindau and breast cancer presented with worsening abdominal and back pain. (a) An enhancing right adrenal mass is noted (black arrow) on the contrast-enhanced CT. Numerous cystic lesions arising from the tail of the pancreas are noted in addition to a microcystic serous cystadenoma (white arrow). (b) A heterogeneously enhancing left renal mass was proven on biopsy to represent a renal cell carcinoma (arrow). Numerous cysts are seen in the right kidney and pancreas consistent with known history of Von Hippel-Lindau (arrowhead). (c) [^{123}I]MIBG scan demonstrates intense radiotracer uptake in the right adrenal gland confirming the diagnosis of pheochromocytoma (arrow).**

are illustrated. This review also explores common metastatic patterns.

Pheochromocytoma and paraganglioma imaging findings

On computed tomography (CT), the typical appearance of a pheochromocytoma or paraganglioma is a mass with an unenhanced density greater than 10 Hounsfield units (HU), avid contrast enhancement due to a rich capillary network, and delayed washout[1] (Fig. 1). Internal hemorrhage can sometimes be seen within the tumor (Fig. 2). Cystic changes, necrosis, and internal calcifications are commonly described[6]. Rarely, these masses show low attenuation or minimal enhancement[1]. By comparison, lipid-rich adrenal adenomas tend to have low density on unenhanced CT (<10 HU) and show early washout[7]. The theoretical risk of precipitating a hypertensive crisis has previously prevented intravenous iodinated contrast administration in individuals with suspected or known pheochromocytomas, however no adverse events were reported in a retrospective study of 25 patients with paragangliomas and pheochromocytomas who received non-ionic iodinated contrast[8]. Contrast has also been used in our practice without any reactions (Fig. 2).

The improved tissue contrast of magnetic resonance imaging (MRI) allows further characterization of adrenal

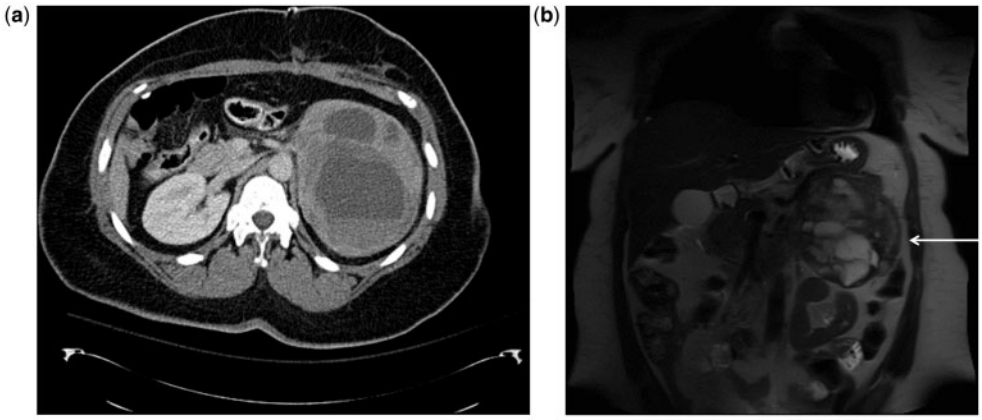

Figure 2 **A 45-year-old man undergoing placement of an adjustable gastric band experienced retroperitoneal bleeding during the procedure secondary to an incidentally discovered mass. Postoperative tests showed increased levels of plasma metanephrine, 24-h urine catecholamines, vanillylmandelic acid, and metanephrines consistent with a diagnosis of pheochromocytoma. (a) Contrast-enhanced axial CT image of the abdomen demonstrates a complex left adrenal mass with thick enhancing walls. There is a central, high density component with fluid levels consistent with internal hemorrhage. (b) Coronal T2-weighted MR image demonstrates a heterogeneous adrenal mass with multiple internal foci of T2 prolongation with septation (arrow).**

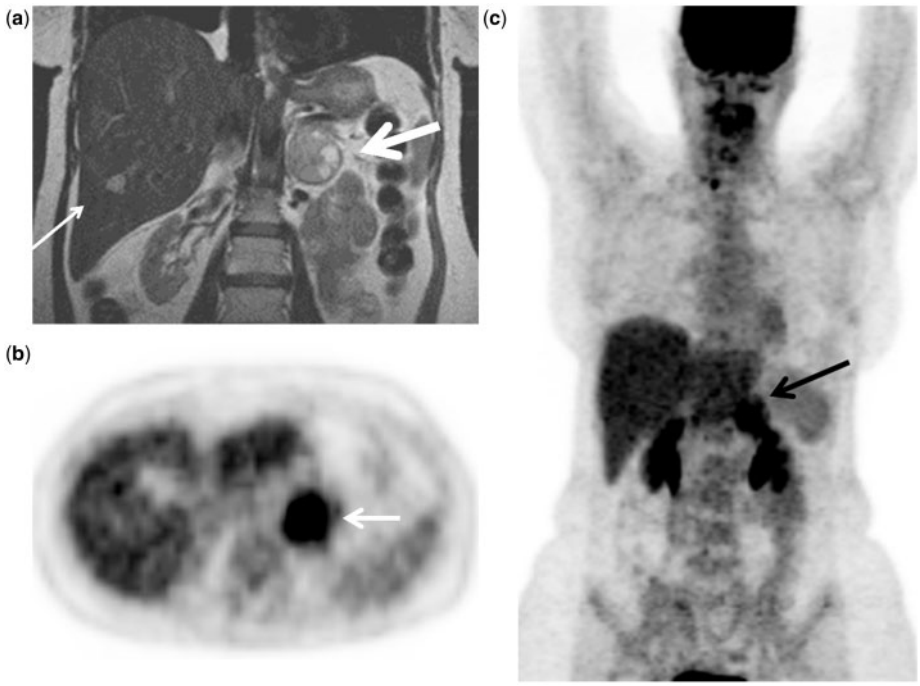

Figure 3 **A 57-year-old woman initially presented with severe left hip and flank pain without a history of trauma. CT demonstrated a left adrenal mass (not available). (a) T2-weighted coronal MRI of the abdomen shows a heterogeneous mass with cystic components arising from the left adrenal gland (thick arrow). A liver cyst is incidentally noted (thin arrow). (b) Axial [^{18}F]FDG-PET image demonstrates FDG uptake in the adrenal mass (arrow). (c) [^{18}F]FDG-PET coronal maximal intensity projection (MIP) again demonstrates the FDG-avid primary left adrenal mass consistent with pheochromocytoma (arrow).**

lesions[9]. In general, pheochromocytomas demonstrate T2 prolongation and variable, although often intense, contrast enhancement resulting in the light bulb sign (Fig. 3)[9]. Up to 35% of pheochromocytomas, however, fail to demonstrate this typical T2 prolongation[9]. Internal hemorrhage and cystic components contribute to the heterogeneous MRI appearance of these tumors. Additional use of opposed phase imaging can be helpful

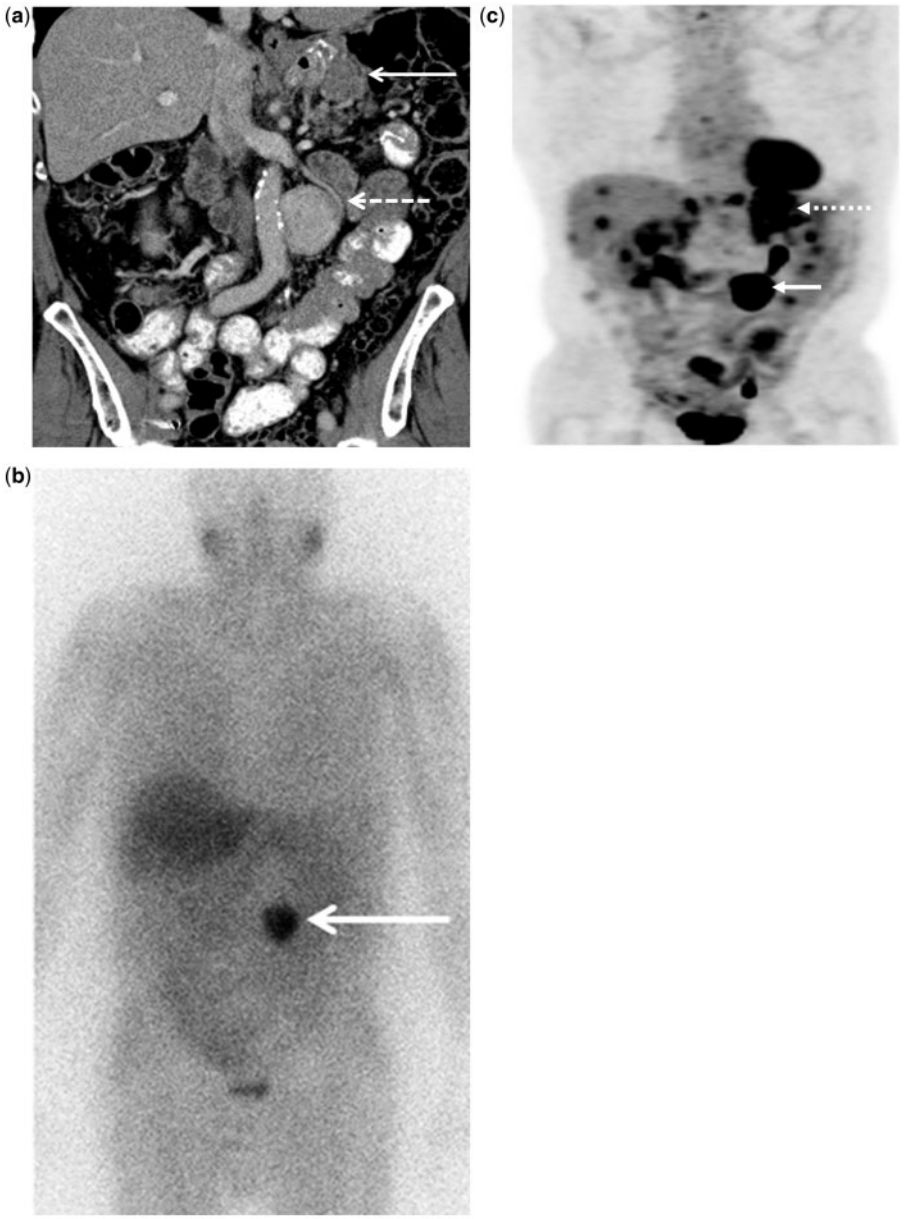

Figure 4 **A 77-year-old man had an adrenal mass incidentally discovered on a restaging scan following resection of a gastrointestinal stromal tumor (GIST). (a) Coronal CT image with oral and intravenous contrast demonstrates a homogeneous, hypodense mass (solid arrow) adjacent to the surgical bed representing local recurrence of GIST. An enhancing retroperitoneal mass adjacent to the aorta corresponded to the location of the sympathetic ganglia and raised the possibility of paraganglioma (dotted arrow). (b) [^{123}I]MIBG scan demonstrates intense radiotracer uptake to the left of midline in the midabdomen corresponding to the previously noted paraganglioma (arrow). The upper abdominal GIST does not demonstrate any radiotracer uptake. Physiologic uptake of [^{123}I]MIBG is noted in the salivary glands, liver, bladder, and bowel. (c) Coronal [^{18}F]FDG-PET MIP shows intense FDG uptake in both the GIST (dotted arrow) and pheochromocytoma (solid arrow) as both tumors are metabolically active. The combination of GIST and paraganglioma is diagnostic of Carney-Stratakis syndrome. Numerous other foci of FDG uptake within the liver and lymph nodes are consistent with metastatic disease.**

as pheochromocytomas and paragangliomas do not exhibit dropout of signal on opposed phase imaging, but many lipid-rich adenomas do[10].

Ideally, the biochemical diagnosis is made before imaging is performed. However, functional imaging with [^{123}I]metaiodobenzylguanidine (MIBG) single photon emission-computed tomography (SPECT), [^{111}In]octreotide SPECT, and positron emission tomography (PET) can be useful to confirm the diagnosis, identify sites of disease, and evaluate metastases. MIBG

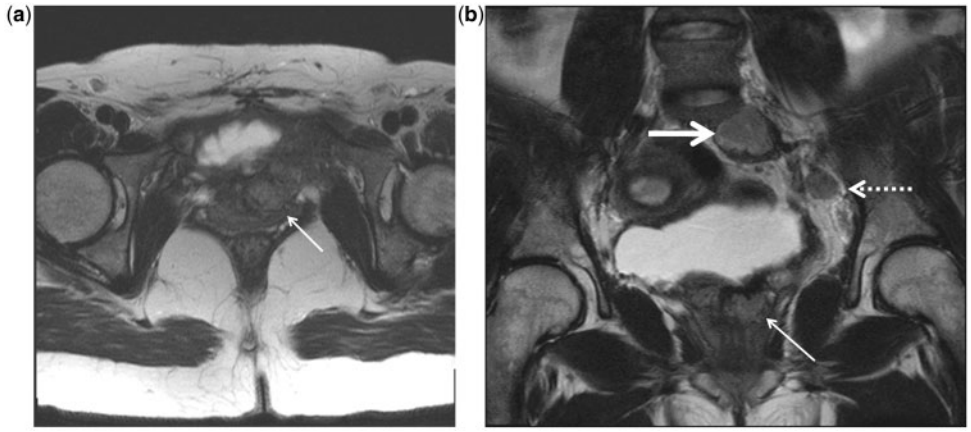

Figure 5 **A 35-year-old woman with a paternal family history of pheochromocytoma was initially diagnosed with paraganglioma at the base of the bladder causing left hydronephrosis and hypertension for which she underwent partial cystectomy and resection of the mass. (a) Axial T2-weighted MRI demonstrates heterogeneous, hyperintense signal at the base of the bladder to the left of midline (arrow) consistent with recurrence. (b) Coronal T2-weighted MRI demonstrates the same mass at the base of the bladder (thin arrow). At the level of the aortic bifurcation, a left of midline mass demonstrates intermediate signal (thick arrow) corresponding to an organ of Zuckerandl paraganglioma. An enlarged pelvic lymph node is seen on the left (dotted arrow).**

is a guanethidine analog that is taken up and stored in vesicles within cells of the sympathomedullary system[11]. Although MIBG can be labeled with either ^{123}I or ^{131}I, ^{123}I is preferred because of the shorter half life, lack of beta emission, and lower radiation dose compared with ^{131}I. [^{123}I]MIBG is also preferred over [^{131}I]MIBG because the use of SPECT improves sensitivity and anatomic localization, whereas the low count rate and high energy collimators needed for ^{131}I makes SPECT more difficult to perform and yields worse image quality[11]. Prior to an [^{123}I]MIBG study, the patient must be screened for medications that could interfere with MIBG uptake, necessitating discussion with the referring clinician. The patient should also receive supersaturated potassium iodide (SSKI) or Lugol solution to block radiotracer uptake in the thyroid[11].

Somatostatin analogs such as octreotide bind to cellular hormonal receptors important for inhibition of neuroendocrine hormone synthesis[11]. The extent of uptake of [^{111}In]octreotide is variable and dependent on the profile/subtypes of somatostatin receptors in the tumor. In patients with an incidental mass that is suspected to be a pheochromocytoma or paraganglioma, the choice of initial imaging radiotracer can be difficult. In general, [^{123}I]MIBG is thought to be slightly more sensitive than [^{111}In]octreotide for the site of primary disease and is often the radiotracer of choice[12]. [^{111}In]octreotide has high sensitivity for metastatic disease and can be positive in tumors that have no MIBG uptake[1,11]. Therefore, if the initial [^{123}I]MIBG scan is negative, an [^{111}In]octreotide scan may be helpful.

Recently, the utility of PET has been investigated. There are several radiotracers that can be used with PET including [^{18}F]fluorodeoxyglucose (FDG), [^{18}F]dihydrozyphenylalanine (DOPA) and [^{18}F]dopamine. Although [^{18}F[FDG-PET has a high sensitivity for metastatic disease, the specificity is generally less than that of [^{123}I]MIBG or [^{111}In]octreotide[11]. To date, PET remains in the realm of investigation playing a predominantly complementary role in the evaluation of this patient population.

Figure 6 **A 51-year-old woman presented with a cough. Axial contrast-enhanced CT through the level of the aortic arch demonstrates an intensely enhancing mediastinal mass in the anterioposterior window (arrow). Surgical pathology confirmed the diagnosis of paraganglioma.**

There is no consensus on the order in which radiologic tests should be performed for patients with suspected neural crest tumors. A biochemical diagnosis is key, although anatomic imaging with CT or MRI and functional imaging with [^{123}I]MIBG SPECT,

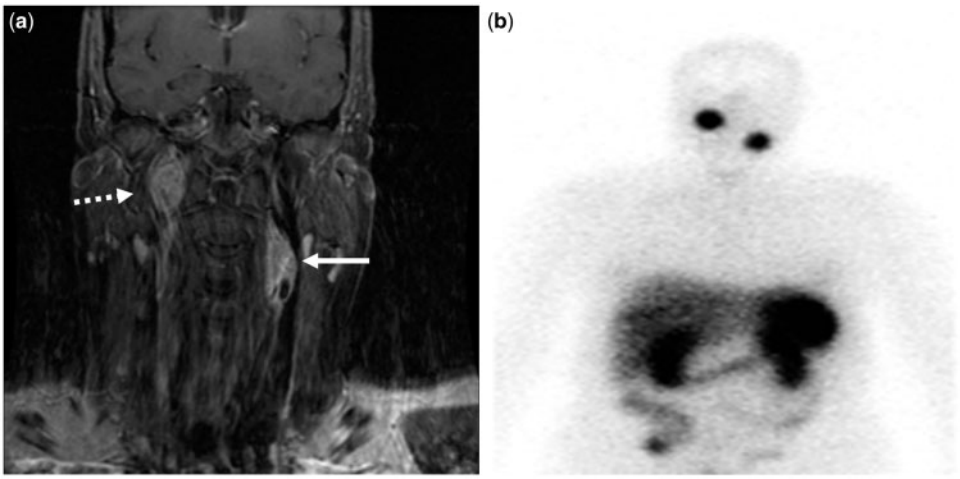

Figure 7 **A 40-year-old woman recently postpartum presented with right-sided neck pain, minimally relieved with standing. (a) Coronal contrast-enhanced T1-weighted MRI demonstrates enhancing masses adjacent to the bilateral carotid arteries inferior to the jugular foramen on the right (dashed arrow) and at the level of the carotid bifurcation on the left (solid arrow). (b) [^{111}In]Octreotide scan shows radiotracer uptake in the bilateral neck masses confirming the diagnosis of paraganglioma.**

[^{111}In]octreotide SPECT and/or [^{18}F]FDG-PET can be helpful in evaluation and staging. Current clinical management relies on a combination of surgical resection, [^{131}I]MIBG therapy, and chemotherapy in malignant tumors.

Hereditary syndromes

Pheochromocytomas and paragangliomas can occur either sporadically or due to germline mutations with at least 9 suspect genes identified[13]. Numerous named genetic syndromes have been associated with pheochromocytoma and paraganglioma. Von Hippel-Lindau (VHL) is an autosomal dominant disease caused by VHL gene mutations that predisposes individuals to central nervous system hemangioblastomas, renal cysts, renal cell carcinoma, pancreatic cysts, retinal angiomas, and pheochromocytomas (Fig. 1). Carney Stratakis syndrome is a rare association of familial paraganglioma and gastrointestinal tumor (Fig. 4). Other associations include multiple endocrine neoplasia (MEN2), neurofibromatosis type I (NF1), Sturge-Weber syndrome, and Carney syndrome[2]. Genetic analysis has also linked mutations in the succinate dehydrogenase (SDH) genes to the development of paranganglioma and pheochromocytomas[2]. At least 4 paraganglioma syndromes named paraganglioma syndrome I–IV have been linked to mutations in the SDHD, SDH5, SDHC, and SDHB, respectively[2]. Recent research suggests that the current list of associated genetic mutations is not yet complete[2].

Extraadrenal sympathetic paraganglioma

Extraadrenal paragangliomas behave more aggressively than their adrenal counterparts with metastases occurring in 20–70% of cases[3,4]. Retroperitoneal paragangliomas are classically associated with the organ of Zuckerandl, the chromaffin paraaortic tissue between the origin of the inferior mesenteric artery and the aortic bifurcation (Fig. 5). Together with the organ of Zuckerandl, the infradiaphragmatic paraaortic region and mediastinum constitute the three most common locations of extraadrenal paragangliomas[4] (Fig. 6). The urinary bladder is another common site of paraganglioma. Catecholamine-secreting tumors in this location can produce any of the typical sympathetic symptoms such as paroxysmal hypertension, tachycardia, headache, perspiration, palpitations, pallor, weight loss, and hyperglycemia in addition to painless hematuria and micturition syncope[14] (Fig. 4).

Extraadrenal parasympathetic paraganglioma

Parasympathetic, nonsecretory paragangliomas in the head and neck are also commonly reported. Tumors in the carotid body, for example, are well known clinical entities associated with a lower rate of metastases than their retroperitoneal counterparts and characteristically described as well-defined soft tissue masses within the carotid space splaying the carotid bifurcation[3,15] (Fig. 7). Other locations for paragangliomas include the glomus jugulare, glomus vagale, and glomus tympanicum.

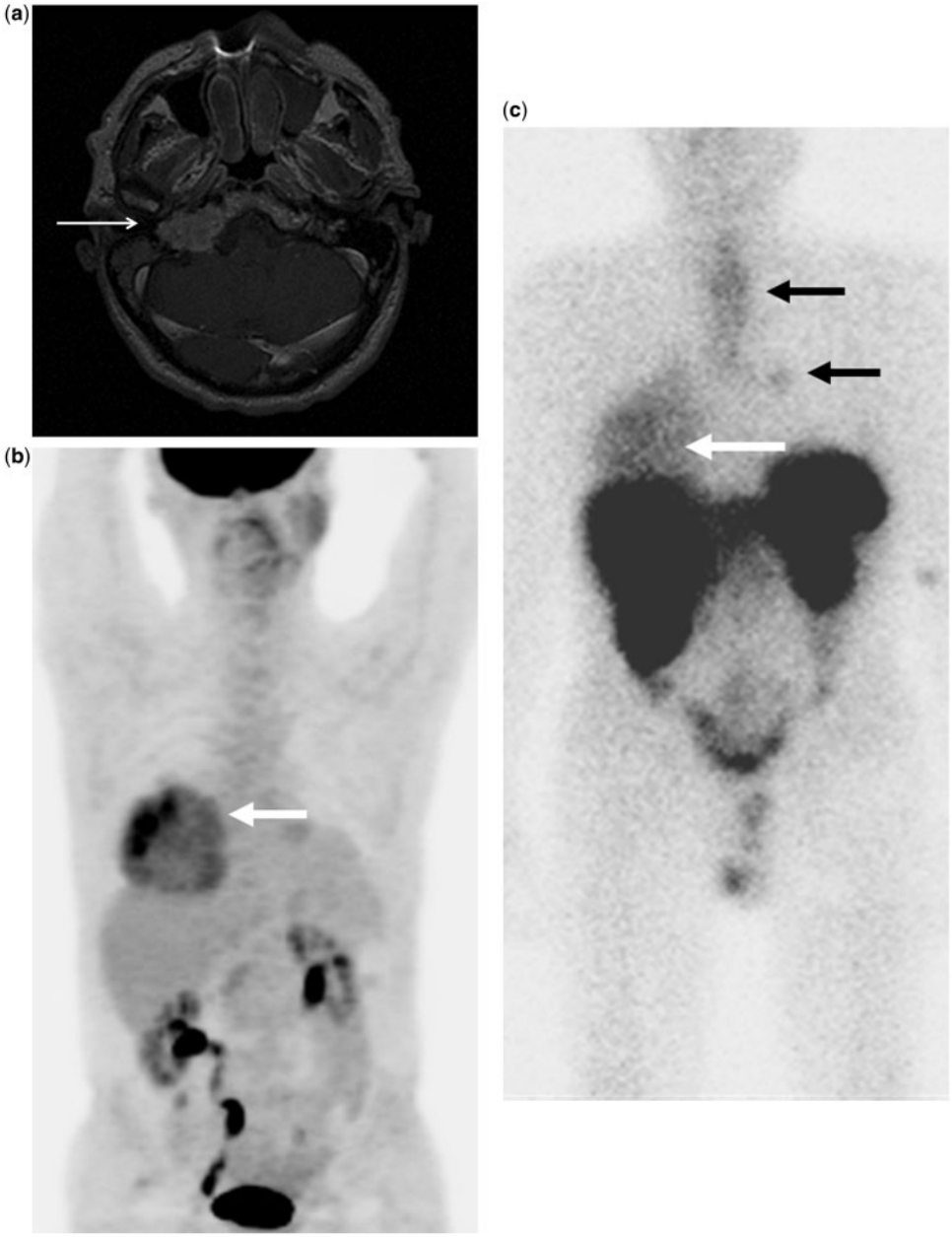

Figure 8 **A 61-year-old man with a history of treated right glomus jugulare and right glomus vagale tumors presented with progressive right facial droop, dysphagia, and right eyelid ptosis. (a) Axial contrast-enhanced T1-weighted MRI demonstrates an enhancing right jugular fossa mass involving the right petrous apex (white arrow) and clivus. The mass extends into the cavernous sinus. (b) Coronal [^{18}F]FDG-PET MIP demonstrates FDG uptake within a right lower lobe mass (arrow). (c) [^{111}In]Octreotide scan demonstrates radiotracer uptake in the right lower lobe (white arrow) compatible with metastases. Uptake was also noted in the mediastinum and bilateral hila consistent with lymphadenopathy (black arrows).**

Glomus jugulare tumors arise from the jugular foramen of the skull base in association with branches from either the vagus or glossopharyngeal nerve. These tumors are locally aggressive with extension into the adjacent bones and intracranial structures but are hormonally silent[15] (Fig. 8).

Metastatic patterns

No reliable histologic features can currently distinguish between benign and malignant tumors. In addition to local recurrence at the site of surgical resection, hematogenous and lymphatic metastases are common[3].

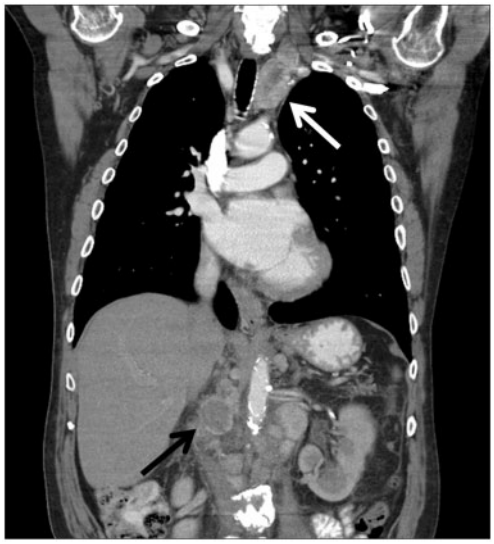

Figure 9 **A 70-year-old man with a history of diabetes and hypertension initially presented with upper abdominal pain. Coronal contrast enhanced CT 1 year after the initial presentation (baseline studies not available) of a paraganglioma demonstrates widely metastatic enhancing mediastinal (white arrow) and retroperitoneal (black arrow) lymph nodes. Some of the lymph nodes are centrally hypodense.**

Metastatic disease is often diagnosed when tumor foci are identified at sites where chromaffin tissue is absent. Common sites of metastatic spread include regional lymph nodes, bone, liver, and lung (Fig. 9). One can evaluate for metastatic disease using multiple imaging modalities including CT, MR, MIBG and PET/CT (Figs. 10 and 11). In addition, osseous metastases from pheochromocytomas and paragangliomas may demonstrate radiotracer uptake on bone scans (Fig. 12).

Conclusion

Clinical suspicion for a pheochromocytoma and paraganglioma often begins with the patient history and is confirmed with biochemical testing. The discovery of a primary enhancing mass in a midline or paramidline location should prompt consideration of neural crest lesions. Locating and staging these tumors requires a combination of anatomic and functional imaging modalities. Although contrast-enhanced MRI was preferred in the past for anatomic imaging due to fear of inducing an adrenal crisis with iodinated contrast, contrast-enhanced CT (using nonionic iodinated contrast) is now considered the best initial anatomic study with MRI reserved

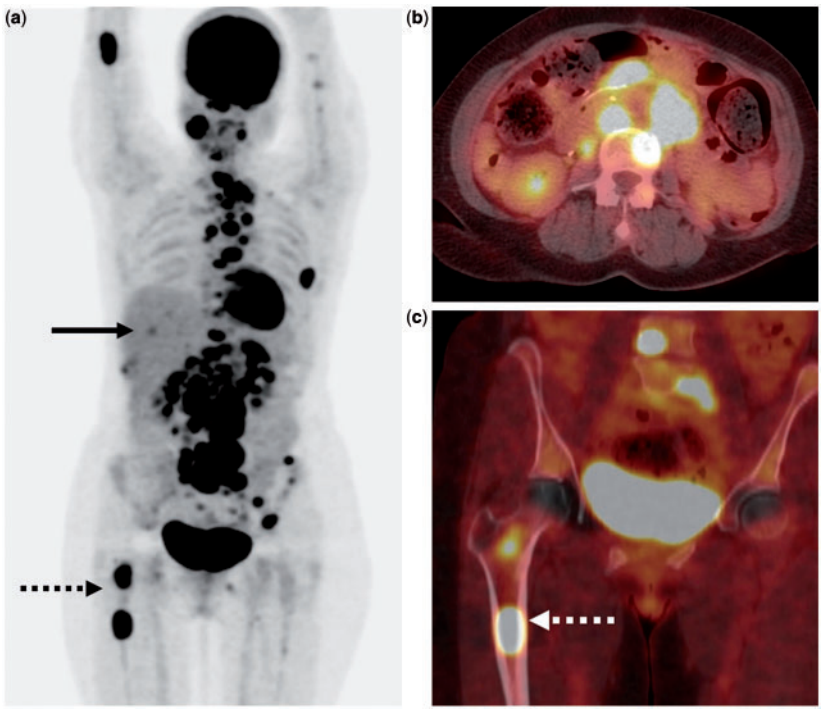

Figure 10 **A 52-year-old woman initially presented with a sensation of mid-epigastric fullness. After initial imaging (not available), the patient underwent surgical excision of a 9-cm abdominal mass with the diagnosis of paraganglioma. (a) Postexcision coronal [^{18}F]FDG-PET MIP demonstrates focal FDG uptake within the frontal bone, liver (solid arrow), femur (dashed arrow), and throughout mediastinal and retroperitoneal lymph nodes consistent with metastatic paraganglioma. (b) Fused axial [^{18}F]FDG-PET/CT illustrates intensely FDG-avid retroperitoneal lymph nodes and a lumbar vertebral body lesion. (c) Fused coronal [^{18}F]FDG-PET/CT demonstrates an intensely FDG-avid right femoral metastasis (arrow).**

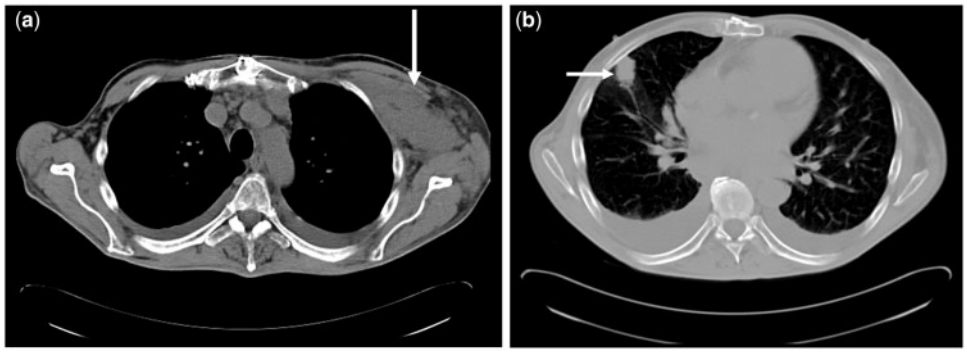

Figure 11 **A 57-year-old man initially presented with episodic sweating and flushing secondary to a right adrenal pheochromocytoma that was resected. One year later, he noticed enlarged cervical lymph nodes that were found to be metastatic pheochromocytoma on biopsy. (a) Axial noncontrast CT image of the upper thorax demonstrates a left subpectoral mass that is slightly hypodense to muscle (arrow). (b) Axial noncontrast CT images show a right middle lobe lung nodule representing metastatic pheochromocytoma (arrow) in addition to bilateral pleural effusions.**

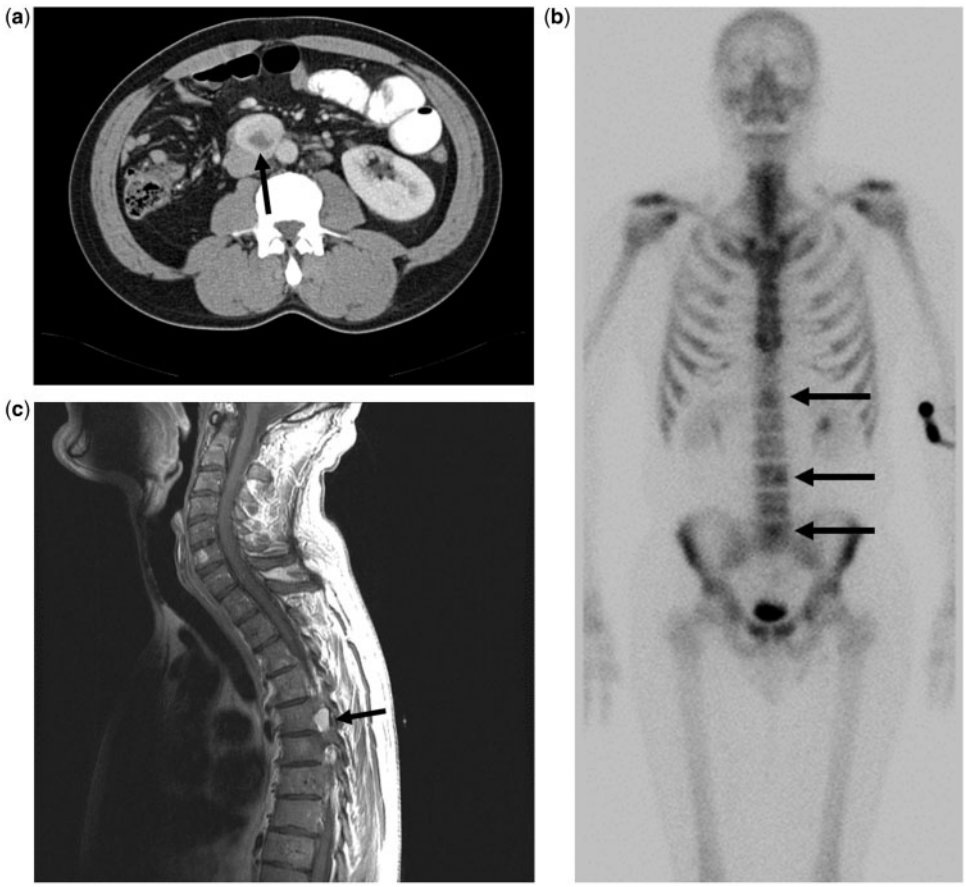

Figure 12 **A 47-year-old man initially presented with abdominal pain. (a) Axial CT scan with oral and intravenous contrast demonstrates an enhancing retroperitoneal mass with central necrosis (arrow). At pathologic examination, this was a paraganglioma. (b) [^{99m}Tc]methylene diphosphonate bone scan performed 2 years after the initial CT demonstrates increased radiotracer uptake in the thoracolumbar spine (arrows). (c) Sagittal T1-weighted MRI with contrast obtained 2 years after the bone scan demonstrates diffuse bone marrow heterogeneity within the vertebral bodies consistent with metastases. An enhancing soft tissue component seen at the level of the T5 vertebral body extends into the right neural foramen and compresses the thecal sac (arrow).**

for problem solving. Functional imaging is often performed concurrently with [^{123}I]MIBG serving as the preferred agent due to its sensitivity and specificity profile[16]. Although these tumors have traditionally been associated with the 10% rule, improved imaging detection and outcome data show that the true story is more complex and prognosis varies depending on the tumor type and location.

References

[1] Blake MA, Kalra MK, Maher MM. Pheochromocytoma; an imaging chameleon. Radiographics 2004; 24: S87–S99. doi:10.1148/rg.24si045506.

[2] Opocher G, Schiavi F. Genetics of pheochromocytomas and paragangliomas. Best Pract Res Clin Endocrinol Metab 2010; 24: 943–956. doi:10.1016/j.beem.2010.05.001.

[3] Wen J, Li HZ, Ji ZG, et al. A decade of clinical experience with extra-adrenal paragangliomas of retroperitoneum; Report of 67 cases and a literature review. Urol Ann 2010; 2: 12–16.

[4] Ayala-Ramirez M, Feng L, Johnson MM. Clinical risk factors for malignancy and overall survival in patients with pheochromocytomas and sympathetic paragangliomas; primary tumor size and primary tumor location as prognostic indicators. J Clin Endocrinol Metab 2011; 96: 717–725. doi:10.1210/jc.2010-1946.

[5] Chrisoulidou A, Kaltsas G, Ilias I, Grossman AB. The diagnosis and management of malignant phaeochromocytoma and paraganglioma. Endocr Relat Cancer 2007; 14: 569–585. doi:10.1677/ERC-07-0074.

[6] Motta-Ramirez GA, Remer EM, Herts BR, Gill IS, Hamrahian AH. Comparison of CT findings in symptomatic and incidentally discovered pheochromocytomas. AJR Am J Roentgenol 2005; 185: 684–688.

[7] Johnson PT, Horton K. Adrenal imaging with multidetector CT; evidence-based protocol optimization and interpretative practice. Radiographics 2009; 29: 1319–1331. doi:10.1148/rg.295095026.

[8] Bessell-Browne R, O'Malley ME. CT of pheochromocytoma and paraganglioma; risk of adverse events with i.v. administration of nonionic contrast material. AJR Am J Roentgenol 2007; 188: 970–974. doi:10.2214/AJR.06.0827.

[9] Varghese JC, Hahn PF, Papanicolaou N, Mayo-Smith WW, Gaa JA, Lee MJ. MR differentiation of phaeochromocytoma from other adrenal lesions based on qualitative analysis of T2 relaxation times. Clin Radiol 1997; 52: 603–606. doi:10.1016/S0009-9260(97)80252-8.

[10] Elsayes KM, Menias CO, Siegel CL, Narra VR, Kanaan Y, Hussain HK. Magnetic resonance characterization of pheochromocytomas in the abdomen and pelvis; imaging findings in 18 surgically proven cases. J Comput Assist Tomogr 2010; 34: 548–553. doi:10.1097/RCT.0b013e3181d529f2.

[11] Intenzo CM, Jabbour S, Lin HC, et al. Scintigraphic imaging of body neuroendocrine tumors. Radiographics 2007; 27: 1355–1369. doi:10.1148/rg.275065729.

[12] Milardovic R, Corssmit EPM, Stokkel Value of ^{123}I-MIBG scintigraphy in paraganglioma. Neuroendocrinology 2010; 91: 94–100. doi:10.1159/000242499.

[13] Yao L, Schiavi F, Cascon A, et al. Spectrum and prevalence of FP/TMEM127 gene mutations in pheochromocytomas and paragangliomas. JAMA 2010; 304: 2611–2619. doi:10.1001/jama.2010.1830.

[14] Siatelis A, Konstantinidis C, Volanis D, Leontara V, Thoma-Tsagli E, Delakas D. Pheochromocytoma of the urinary bladder; report of 2 cases and review of literature. Minerva Urol Nefrol 2008; 60: 137–140.

[15] Rao AB, Koeller KK, Adair CF. From the archives of the AFIP. Paragangliomas of the head and neck; radiologic-pathologic correlation. Armed Forces Institute of Pathology. Radiographics 1999; 19: 1605–1632.

[16] Jacobson AF, Deng H, Lombard J, Lessig HJ, Black RR. ^{123}I-meta-iodobenzylguanidine scintigraphy for the detection of neuroblastoma and pheochromocytoma; results of a meta-analysis. J Clin Endocrinol Metab 2010; 95: 2596–2606. doi:10.1210/jc.2009-2604.